

Effect of electrochemical cycling on microstructures of nanocomposite silicon electrodes using hyperpolarized ^{129}Xe and ^7Li NMR spectroscopy

Special Collection: [Commemorating the Career of David Arthur Shirley](#)

Youngang Mao; Naba K. Karan ; Ravi Kumar; Russell Hopson; Pradeep R. Guduru; Brian W. Sheldon; Li-Qiong Wang 



Journal of Vacuum Science & Technology A 40, 043203 (2022)

<https://doi.org/10.1116/6.0001768>



CrossMark

Related Content

Toward C 13 hyperpolarized biomarkers produced by thermal mixing with hyperpolarized X 129 e

J. Chem. Phys. (July 2009)

Hyperpolarized NMR in Single-File Nanotubes

AIP Conference Proceedings (March 2011)

Room temperature "optical nanodiamond hyperpolarizer": Physics, design, and operation

Rev Sci Instrum (February 2020)



Instruments for Advanced Science

- Knowledge
- Experience
- Expertise

[Click to view our product catalogue](#)

Contact Hiden Analytical for further details:
www.HidenAnalytical.com
info@hiden.co.uk

Gas Analysis

- dynamic measurement of reaction gas streams
- catalysis and thermal analysis
- molecular beam studies
- dissolved species probes
- fermentation, environmental and ecological studies

Surface Science

- UHV TPD
- SIMS
- end point detection in ion beam etch
- elemental imaging - surface mapping

Plasma Diagnostics

- plasma source characterization
- etch and deposition process reaction kinetic studies
- analysis of neutral and radical species

Vacuum Analysis

- partial pressure measurement and control of process gases
- reactive sputter process control
- vacuum diagnostics
- vacuum coating process monitoring

Effect of electrochemical cycling on microstructures of nanocomposite silicon electrodes using hyperpolarized ^{129}Xe and ^7Li NMR spectroscopy

Cite as: J. Vac. Sci. Technol. A 40, 043203 (2022); doi: 10.1116/6.0001768

Submitted: 24 January 2022 · Accepted: 22 April 2022 ·

Published Online: 18 May 2022



View Online



Export Citation



CrossMark

Youngang Mao,¹ Naba K. Karan,^{a)} Ravi Kumar,² Russell Hopson,¹ Pradeep R. Guduru,² Brian W. Sheldon,² and Li-Qiong Wang^{1,b)}

AFFILIATIONS

¹Department of Chemistry, Brown University, Providence, Rhode Island 02912

²School of Engineering, Brown University, Providence, Rhode Island 02912

Note: This manuscript is a part of the Special Topic Collection Commemorating the Career of David Arthur Shirley.

a) Present address: The Center for Clean Energy Engineering, University of Connecticut, Storrs, CT 06269.

b) Author to whom correspondence should be addressed: Li_Qiong_Wang@Brown.edu

ABSTRACT

The microstructural stability of composite electrodes during electrochemical cycling is critically important as it dictates the performance of Li-ion batteries. The issue becomes even more important for the high capacity alloying anode such as silicon that typically exhibits dramatic lithiation–delithiation-induced volume changes. The solid electrolyte interphase (SEI) layer formed on the active electrode surface has a profound effect on the overall microstructural stability of composite electrodes. An ideal SEI layer allows Li^+ ions in and out of the electrode, but is an insulator to electrons, preventing the electrolyte from being further reduced. However, the SEI layers formed during initial lithiation may experience changes or degradation with subsequent cycling, adversely affecting the electrode performance. A combination of hyperpolarized ^{129}Xe and ^7Li nuclear magnetic resonance spectroscopies was applied to probe the microstructures of nanocomposite silicon electrodes at various stages of the lithiation–delithiation cycle. The results obtained from this study shed light on the degradation mechanism of nanocomposite Si electrodes upon electrochemical cycling and should prove useful in the effort to design more robust electrodes in the future.

Published under an exclusive license by the AVS. <https://doi.org/10.1116/6.0001768>

I. INTRODUCTION

The Li-ion battery has attracted a lot of attention as it is commonly used in portable electronics and electric vehicles. Much effort has been devoted recently to developing advanced anode and cathode materials to enhance the performance of the Li-ion battery and expand its application. Silicon is one of the most promising anode materials for Li-ion batteries due to its high volumetric and specific capacity.¹ However, huge volumetric changes^{1,2} during electrochemical cycling affect the integrity and stability of the silicon anode, dramatically reducing the cycle life of the battery and limiting its wider application. Nanostructuring of Si electrodes has been demonstrated to be an effective strategy in mitigating the

lithiation–delithiation-induced strain that significantly improves their cyclability.^{3,4} The cycle life and stability of Si-based electrodes were further improved by using binders that effectively glue the active particles and conducting agents (e.g., super P carbons) together and to the current collectors.^{5–13} The stability of the solid electrode interface (SEI) layer is another key factor that affects the performance and cycle life of the battery. The SEI layer is a film formed as a result of electrolyte reduction on the surface of the anode during the initial lithiation. An ideal SEI layer should be a good conductor for Li^+ ions, allowing Li^+ ions in and out of the electrode, but an insulator to electrons, preventing the electrolyte from being further reduced. Microstructures of nanocomposite Si electrodes including the

05 September 2023 11:38:23

thickness of the SEI layer, pores, and connectivity of the pores most likely experience changes during cycling resulting from SEI formation and cracking/agglomeration of nanoparticles during cycling. In general, these changes negatively impact the performance and lifetime of the battery. Thus, it is critically important to examine the changes in microstructures of nanocomposite electrodes to better understand the stability of the SEI and the integrity of the electrodes to further improve the capacity and cycle life of the Li-ion battery.

Numerous studies have been reported on the morphology and chemical composition of the SEI layer formed on silicon nanoparticle composite anodes using a variety of microscopy and spectroscopic techniques.^{14–21} The thickness of SEI layers was estimated based on the transmission electron microscopy (TEM) images for the Si nanoparticle electrode upon cycling.¹⁴ However, it is challenging for TEM to differentiate between the SEI layer and lithiated Si nanoparticles to provide accurate results. In addition, the aforementioned techniques^{14–21} were not applicable for obtaining the information on the (nano)porosity and connectivity of (nano)pores in the Si nanocomposite electrodes. Since microstructures of pores and the connectivity of the pores significantly influence the ion transport properties in nanocomposite Si electrodes, impacting the overall Li-ion battery energy output, it is important to examine the changes in (nano)porosity and connectivity among (nano)pores before and after electrochemical cycling to better design next generation of Li-ion batteries. Hyperpolarized (HP) ¹²⁹Xe NMR has been proven to be a powerful tool for probing (nano)pores and their connectivity^{22,23} due to a large chemical shift range of ¹²⁹Xe, which is extremely sensitive to the local chemical environment and microstructure of the pores.^{23–28} The dramatic increase in signal to noise (a factor of 10⁴) by employing the optical pumping method to produce HP xenon enables pore characterization studies without using high pressured Xe gas. Our previous study²⁹ has already demonstrated that HP ¹²⁹Xe NMR is a unique tool for probing changes in porosity and connectivity among the pores in nanoporous composite Si electrodes as a result of the formation of the SEI layer. In this study, HP ¹²⁹Xe NMR is applied to examine changes in microstructures of Si (nano)composite electrodes including the thickness of the SEI layer, uniformity of the (nano)pores, and connectivity among the (nano)pores as a result of electrochemical cycling. Due to the complex nature of the Xe interactions with the surface, comparative studies of ¹²⁹Xe NMR spectra taken before and after electrochemical cycling were conducted, enabling the examination of the electrochemical cycling effect on the microstructures of electrodes. In comparison with the previous study²⁹ on electrodes without electrochemical cycling, this work provides new insights into how electrochemical cycling affects the porosity, pore connectivity, and the thickness of SEI layers in nanocomposite Si electrodes. The information obtained from this study is critically important for gaining a better understanding of the mechanism of disintegration of the nanocomposite silicon electrodes and degradation of the SEI upon electrochemical cycling that will help build robust batteries in the future.

II. EXPERIMENT

A. Sample preparation

The composite anode is made of Si nanoparticles (~20 nm in diameter), conductive carbon (super P), and carboxymethyl

cellulose (CMC) binder that were purchased from Sigma Aldrich. Si (nano)particles were mixed with carbon (super P) with a weight ratio of 1 to 1 in ethanol. The (Si + C) mixture was stirred for 4 h and sonicated for 2 h at room temperature, followed by drying on a hotplate at 100 °C for 15 h with continuous stirring. The mixed powder was placed in an oven at 100 °C for additional 9 h of drying. To make laminated composite Si electrodes (Si + C + CMC), the dried powder mixture (Si + C) was added to 2 wt. % CMC solution in water [the amount of CMC solution is determined by the ratio of (Si + C):CMC fixed at 80:20 by weight] followed by stirring for 30 min and the resulting slurry was then cast on the copper foil and dried under vacuum at 100 °C for several hours.

The electrochemical cycling was performed in a beaker cell. Beaker cells were assembled with a circular 2-in. diameter anode disk that was cut out from the composite electrode laminate serving as a working electrode and lithium metal foil serving as a reference electrode using the conventional liquid electrolyte that was made of 1 M LiPF₆ (lithium hexafluorophosphate) dissolved in a 1:1:1 ethylene carbonate/diethyl carbonate/dimethyl carbonate (DMC) solvent mixture. The formation of SEI on the Si nanocomposite electrode was carried out using this beaker cell by holding the working electrode at a constant potential (0.5 V versus Li/Li⁺) for 12 h. The electrochemical measurements including cell assembly and cycling were conducted in an Ar-filled glove box (H₂O < 0.1 ppm and O₂ < 0.1 ppm). Cycling was performed galvanostatically using a constant rate of C/20 at room temperature. A reference sample (soaked only) was also prepared by simply immersing the electrode laminate in the electrolyte solution for 12 h without applying any potential. Two cycled samples, denoted as CYC1 and CYC2, were prepared after one and five lithiation–delithiation cycles, respectively. Cycled composite electrodes after cycling were taken out from the beaker cell and thoroughly rinsed with DMC followed by natural drying overnight in an Ar-filled glove box. NMR samples were prepared from the dried samples by gently scraping off from the copper disk and packing them into a 7 mm Zirconia rotor in an Ar-filled glove box. The entire process of cell disassembly, active anode material scrapping, drying, and NMR sample preparation was carried out in an Ar-filled glove box, and the NMR spectra were taken within 15–20 h. Care was taken to avoid sample exposure to the environment and as such we do not anticipate additional microstructural changes in the cycled samples after electrochemical tests were done.

B. Hyperpolarized ¹²⁹Xe NMR measurements

HP ¹²⁹Xe NMR experiments were carried out on a Bruker Avance DSX 300 MHz spectrometer operating at 82.98 MHz (magnetic field 7.05 T) with a variable temperature magic angle spinning double-resonance probe. The HP ¹²⁹Xe gas produced using a homemade ¹²⁹Xe polarizer constructed based on the previous study by the Hersman and Saam groups^{30–32} was introduced into the packed samples through a small-drilled hole in the rotor cap via plastic tubing (1.5 mm ID). For HP ¹²⁹Xe NMR experiments, a single-pulse Bloch-decay method was used and samples were loaded into 7 mm Zirconia rotors inside the Ar glove box. The rotor cap with a small-drilled hole allowed the HP ¹²⁹Xe gas to

05 September 2023 11:38:23

pass through a plastic capillary tube into the sample. The HP ^{129}Xe NMR experiments were performed without sample spinning. The HP ^{129}Xe NMR spectra were taken with a $1\text{-}\mu\text{s}$ ^{129}Xe pulse, a 10 ms repetition delay, and under a continuous flow (CF) of HP xenon. The number of transients was 500–2000 depending on the signal to noise. A gas mixture of Xe, He, and N_2 of 1%:66%:33% in volume was used in HP ^{129}Xe gas production for all CF HP ^{129}Xe NMR measurements, while a constant flow rate of ~ 300 cc/min (gas flow normalized to standard conditions) was maintained. A liquid N_2 cooling assembly and temperature controller attached to the NMR probe allowed variable temperature NMR measurements carried out. The chemical shift for the free xenon gas was assigned to 0 ppm as a reference for all ^{129}Xe NMR chemical shift data.

C. ^7Li NMR measurements

Solid-state ^7Li NMR measurements were carried out with a Bruker Avance DSX 300 MHz spectrometer (7.05 T magnetic field and 116.64 MHz resonance frequency) using a magic angle spinning double-resonance probe. The experiments were carried out without magic angle spinning. Single-pulse NMR spectra were collected with a pulse length of $4\text{ }\mu\text{s}$ (90° pulse) for ^7Li and a repetition delay of 200 ms. The number of transients was 4096. Li NMR chemical shifts were referenced by 1 M LiCl solution in D_2O at 0 ppm.

III. RESULTS AND DISCUSSION

A. HP ^{129}Xe NMR at 300 K

HP ^{129}Xe NMR measurements were performed on five Si nanocomposite electrodes: unsoaked, soaked, SEI, CYC1 (cycled one time), and CYC2 (cycled five times) for studying the influence of cycling on microstructures of nanocomposite Si electrodes. Figure 1 displays the CF HP ^{129}Xe NMR spectra taken at 300 K for all five composite electrodes. All spectra taken under the same conditions enabled the examination of any changes in microstructures (the thickness of SEI, pore uniformity, and pore connectivity) upon cycling.

As described in our previous study,²⁹ ^{129}Xe NMR chemical shifts are very sensitive to the local environment of the Xe atom. The measured ^{129}Xe NMR chemical shift, δ_{obs} , for adsorbed xenon is the weighted average of different local environments sampled by xenon atoms within its characteristic diffusion distance,^{24,31}

$$\delta_{obs} = \sum_{i=1, \dots, n} p_i \times \delta_i, \quad (1)$$

where δ_i , p_i , and n represent the chemical shift of xenon adsorbed on site i , the fraction of xenon atoms in site i , and the total number of sites, respectively. The chemical shift in a site (δ_i) can be described as a sum of three components: $\delta_i = \delta_0 + \delta_S + \delta_{\text{Xe-Xe}}$ for porous materials with no paramagnetic impurities nor with strong adsorption centers present. δ_0 is the chemical shift of xenon gas at zero pressure, which is set to 0 ppm as a reference chemical shift, while δ_S , a characteristic of a given adsorption site, is the contribution due to the interaction of Xe with the specific surface site. The δ_S value reflects both the chemical composition of the surface and the geometry of the xenon environment in a given adsorption site.

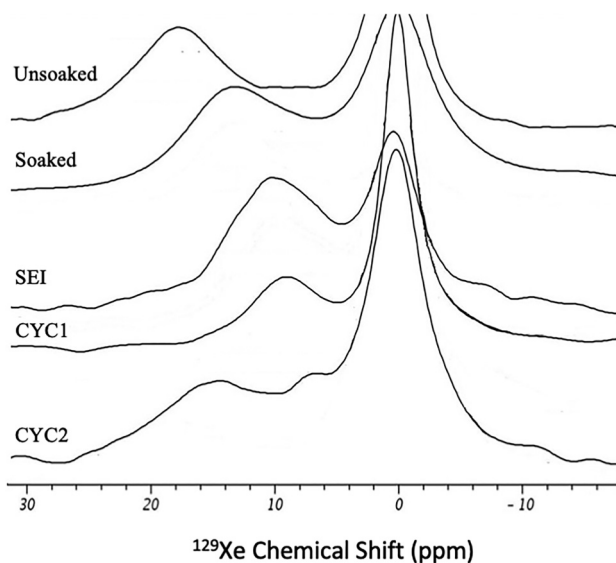


FIG. 1. CF HP ^{129}Xe NMR spectra taken at 300 K for samples of unsoaked, soaked, SEI, CYC1 (cycled one time), and CYC2 (cycled five times) composite electrodes. The peaks at 0 ppm are cut off due to the vertical expansion of the spectra.

$\delta_{\text{Xe-Xe}}$ comes from the Xe–Xe interactions that are dependent on xenon concentration. However, the contribution from the Xe–Xe interactions, $\delta_{\text{Xe-Xe}}$, is negligible in the present study due to the very low concentration of Xe in the sample since only a very low partial pressure of xenon (1% of total or 10 mbar) was used in the CF gas mixture. The enhancement of the Xe NMR signal by several orders of magnitude was achieved through optical pumping of Xe gas and subsequent spin-exchange between Rb excited electronic spin states and Xe nuclear spin states. This spin-exchange results in a nonequilibrium population in Xe spin states, which dramatically increases the ^{129}Xe NMR signals, enabling the use of low Xe concentration in the measurement. Thus, the measured HP ^{129}Xe NMR signals at the chemical shift δ_{obs} mostly from the interaction of Xe with the surface of porous materials rather from the Xe–Xe interaction. The spin-polarized Xe gas percolates through the connected pores and samples local pore environments, registering a chemical shift that correlates with pore size. ^{129}Xe NMR has the unique advantage of probing not only these buried interfaces but also the connectivity between pores as compared with other techniques.³² From the comparative studies of a series of HP ^{129}Xe NMR spectra taken under the same conditions, it is possible to obtain information on the thickness of the SEI (related to the pore size of the voids created among nanoparticles), uniformity of the pores (distribution of different types of pores), and connectivity among pores.

A resonance peak at 0 ppm in Fig. 1 is assigned to the free Xe gas that was trapped in the free space inside the rotor and above the packed samples, and the peaks with larger or positive chemical shifts are associated with the adsorbed Xe within the pores of the sample material. Although the data were taken for “unsoaked,”

“soaked,” and “SEI” samples previously,²⁹ the measurements were repeated on freshly prepared samples under the same condition as for the CYC1 and CYC2 samples to examine any microstructural changes arising from electrochemical cycling in this study. Figure 1 displays obvious changes in chemical shifts for the adsorbed Xe resonance peaks after SEI formation and electrochemical lithiation/delithiation cycling. The chemical shift for the soaked sample is shifted to a lower value after immersing a dry composite electrode into the electrolyte solution. Additionally, the chemical shift for the SEI sample is further shifted to a lower value as compared with soaked sample. These observations are in agreement with our previous report.²⁹ The resonance peaks in ¹²⁹Xe NMR spectra at higher chemical shifts are often associated with the smaller pores when the surface chemical composition and geometry of the pores are similar. This is because the Xe atom inside the smaller pores has a higher probability (or larger p_i) to be adsorbed onto the surface, resulting in a higher chemical shift as indicated in Eq. (1). A lower chemical shift observed for the SEI sample compared to that of the soaked sample suggests an increase in average pore size in the composite electrode upon SEI formation, presumably arising from nanoparticle agglomeration. Furthermore, similar chemical shifts observed for SEI and CYC1 samples (Fig. 1) suggest that the particle sizes or SEI layer were not significantly affected after one lithiation–delithiation cycle. However, obvious changes in chemical shifts after multiple lithiation–delithiation cycles (compare CYC2 and CYC1 spectra) were observed in Fig. 1, where two ¹²⁹Xe NMR peaks were observed for the adsorbed Xe on CYC2 sample but only one peak for the CYC1 sample. The existence of two ¹²⁹Xe NMR resonance peaks indicates that there are at least two different pore environments for adsorbed Xe in the CYC2 sample. A ¹²⁹Xe NMR peak at 14.5 ppm, an increase of ~5.0 ppm as compared with the peak at ~9.5 ppm for the CYC1 sample suggests that smaller pores are formed, whereas an additional resonance peak at ~6.5 ppm is indicative of the presence of much larger pores after five cycles. The appearance of a large peak at 6.5 ppm may imply the thickening of SEI layers upon multiple cycling, which causes the particle size to further increase. Consequently, the space between the particles becomes even larger. The broad Xe peak at 14.5 ppm in the CYC2 spectrum with a chemical shift larger than the SEI sample peak (~9.5 ppm) indicates probable mechanical damage (cracking) of the initially formed SEI layer after multiple cycling. The repetitive expansion (lithiation) and contraction (delithiation) of Si nanoparticles are likely to cause small voids or cracks in the SEI layer.

B. ⁷Li NMR at 300 K

⁷Li NMR spectra of unsoaked, soaked, SEI, CYC1, and CYC2 samples are shown in Fig. 2. The ⁷Li NMR spectra were taken at 300 K and under identical conditions for all samples. No ⁷Li NMR peak was present in the unsoaked sample as shown in Fig. 2 because the electrode only consisted of Si, C, and CMC. But a weak ⁷Li NMR peak appeared for the soaked sample despite being washed and dried before the measurement. The observed weak ⁷Li peak suggests the existence of a small amount of Li on the electrode surface. This seems to suggest that SEI may be formed even by just

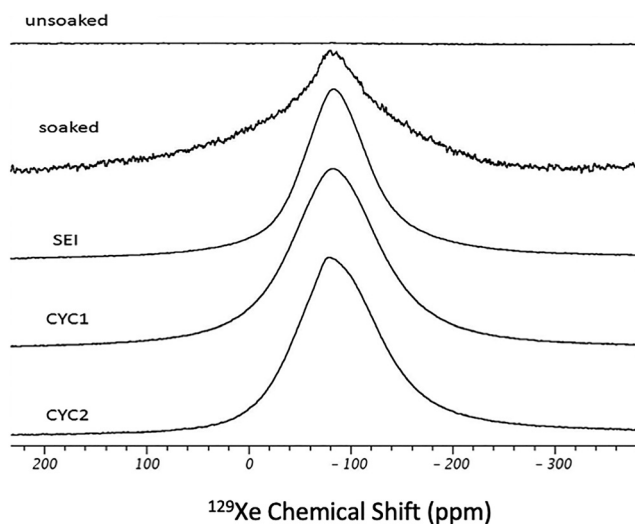


FIG. 2. ⁷Li NMR spectra taken at 300 K for samples of unsoaked, soaked, SEI, CYC1 CYC1 (cycled one time) and CYC2 (cycled five times) composite Si electrodes.

soaking the composite electrode in the electrolyte. A very weak Li signal indicates that the SEI layer developed upon simple soaking of the composite electrode in the electrolyte was not fully formed. Figure 2 clearly illustrates that the Li signal intensities increased significantly upon SEI formation and lithiation–delithiation cycles (compare SEI, CYC1, and CYC2 spectra), implying the formation of thicker SEI layers on these samples. Although ⁷Li NMR is highly sensitive to the amount of Li on electrodes, it is insensitive to identify different local chemical environments of Li⁺ in SEI because of the very wide spectrum linewidth (>100 ppm) caused by a large quadrupole moment of ⁷Li.

The peak intensity ratios of ⁷Li⁺ NMR spectra normalized to the peak intensity of CYC2 are listed in Table I. The order of the intensity of the ⁷Li⁺ NMR peak is SEI = CYC1 < CYC2. The higher intensity of Li⁺ for the CYC2 sample indicates higher lithium content in the CYC2 sample (as part of the SEI), which is consistent with the result from HP ¹²⁹Xe NMR spectra (Fig. 1), where the Xe chemical shifts for SEI and CYC1 samples are the same, but very different from that of the CYC2 sample. It seems likely that a thicker SEI layer is formed in CYC2 than in CYC1 and SEI samples as suggested by both ⁷Li NMR and HP ¹²⁹Xe NMR spectra.

TABLE I. Peak intensity ratios of ⁷Li⁺ NMR spectra normalized to the peak intensity of CYC2.

Samples	Li ⁺ intensity ratios
Soaked	31.33/734.67 = 0.042
SEI	468.51/734.67 = 0.6377
CYC1	450.50/734.67 = 0.6132
CYC2	734.67/734.67 = 1.000

05 September 2023 11:38:23

C. Temperature-dependent HP ^{129}Xe NMR

Temperature-dependent ^{129}Xe NMR has been proven to be a useful tool in probing the dynamics of adsorbed xenon and the morphology of the pore space.^{33–35} A series of temperature-dependent HP ^{129}Xe NMR spectra for all five samples are displayed in Figs. 3 and 4. The temperature-dependent data were measured using a variable temperature probe at temperatures from 170 to 313 K with a 20 K increment. Figures 3 and 4 exhibit the peak associated with adsorbed ^{129}Xe NMR resonance progressively moves to higher chemical shift values with decrease temperature. This shift to the higher ppm values is due to the increased contribution from the adsorbed Xe at lower temperatures.³⁵ In general, the line widths of the ^{129}Xe NMR resonance peak at low temperatures are correlated with the nonuniformity of the pores with no large chemical

shift anisotropy present. The linewidths observed from this study are much narrower than the predicted linewidth associated with the chemical shift anisotropy,^{29,36} suggesting that there is negligible chemical shift anisotropy present in all our samples. Thus, the linewidth at a lower temperature can be used to assess the uniformity of the pores in this study. Broader ^{129}Xe NMR resonance peaks observed for all five samples at lower temperatures arise from the slowing down the exchanges of Xe in pores with different sizes, revealing the nonuniform distribution of the pores. With increasing temperature, the contribution from the adsorbed Xe is reduced and the Xe has high mobility to move through connected pores, resulting in a narrower linewidth. The NMR resonance spectra taken at high temperatures reflect not only a distribution of the pores but also the connectivity among the pores. Therefore, a thorough

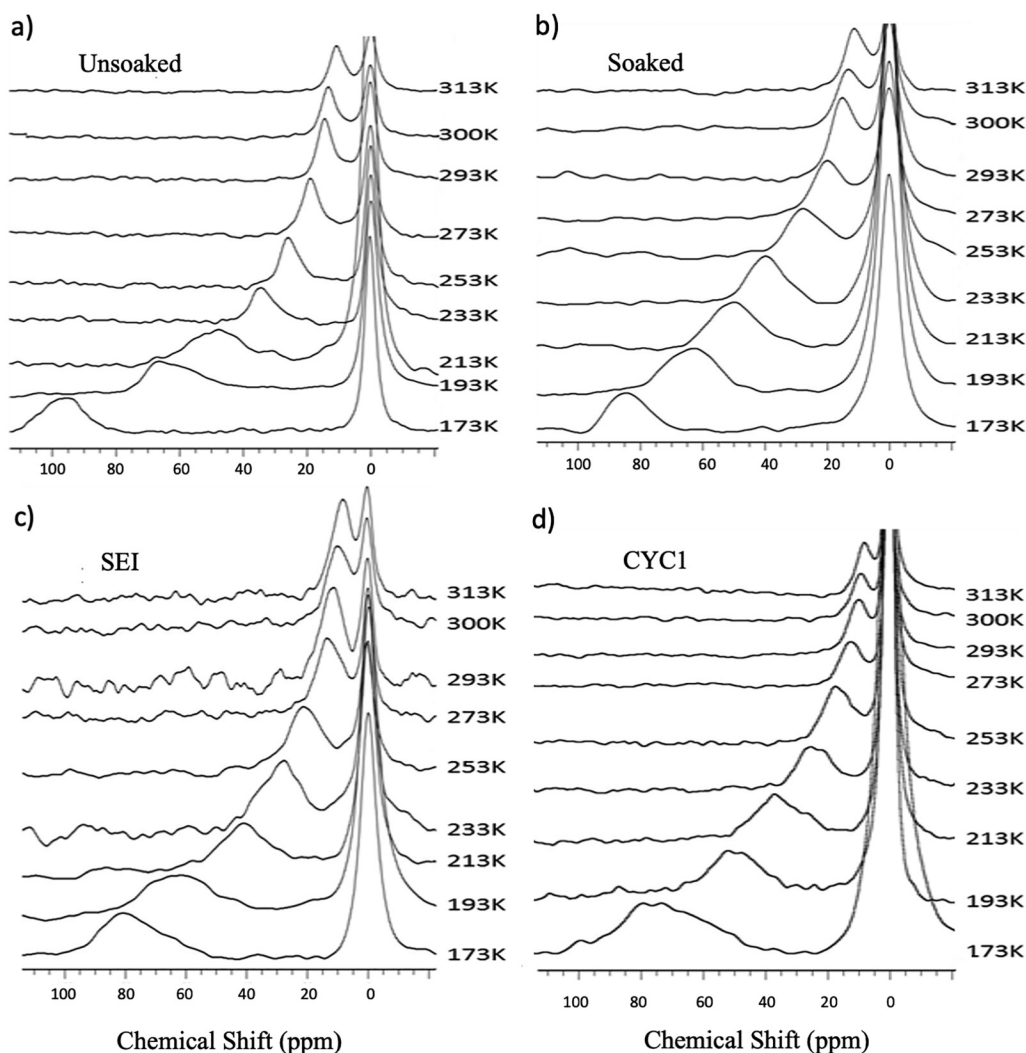


FIG. 3. Temperature-dependent HP ^{129}Xe NMR spectra taken for (a) unsoaked, (b) soaked, (c) SEI, and (d) CYC1 (cycled one time) composite Si electrodes.

05 September 2023 11:38:23

analysis of the linewidths from the temperature-dependent ^{129}Xe NMR data allows us to examine not only the uniformity of the pores environments but also the connectivity among different pores.

Figure 3 shows that the chemical shifts for the unsoaked sample are higher than those for the soaked samples at all temperatures (about 10 ppm difference at 173 K and 5 ppm at 300 K). A previous study on MCM 41 also reported a downward shift in chemical shifts upon molecular adsorption¹⁴ owing to the removal of the micropores or smoothing of the “roughness” of the internal pore surface upon filling in those micropores and rough surfaces with small molecules. It seems that the reduction in a chemical shift for the soaked sample as compared with the unsoaked sample is most likely due to the adsorption of electrolyte molecules or ions onto the nanocomposite Si electrode surface. This downward trend in chemical shifts continues as the SEI layer is formed on the soaked sample (>4 ppm difference at a temperature below 300 K). However, less obvious differences in chemical shifts between SEI and CYC1 samples were observed in comparison to those between the soaked and unsoaked samples. Quite comparable temperature-dependent variation in ^{129}Xe NMR chemical shifts and linewidths for CYC1 and SEI samples in Fig. 3 suggests that the degree of nonuniformity of the pore environments and connectivity among the pores in SEI samples did not change much after one lithiation–delithiation cycle. This is in agreement with the observation of nearly identical chemical shifts at 300 K for SEI and CYC1 samples in Fig. 1 and further suggests that the first delithiation cycle has a negligible effect on the thickness of the SEI layer and does not cause major cracks in the SEI layer since the chemical shifts are altered by the thickening of the SEI layer (larger pores) and the formation of cracks (smaller pores) in the SEI layer. The narrower

peaks at high temperatures observed for both SEI and CYC1 samples suggest that the pores with different pore environments are well connected.

Figure 4 exhibits the temperature dependence of HP ^{129}Xe NMR spectra of the nanocomposite Si electrode after five lithiation–delithiation cycles (CYC2). Corresponding data shown in Fig. 3 for the CYC1 sample (i.e., after one lithiation–delithiation cycle) shown in Fig. 3 are also included in the figure for ease of comparison. In comparison with the spectra for the CYC1 sample, obvious changes in the ^{129}Xe NMR spectrum were observed for the CYC2 sample that underwent multiple lithiation–delithiation cycles. For the CYC2 sample, two resonance peaks are clearly present at temperatures of 193 K and above. This additional peak emerged as a shoulder peak at 193 K and became better resolved at temperatures above 293 K. In contrast, for the CYC1 sample, one single ^{129}Xe NMR peak associated with the adsorbed Xe is present at all temperatures. In addition, the chemical shift values associated with the smaller pores for the CYC2 sample are significantly higher than those for the CYC1 sample (difference of 15 ppm at 173 K and 5 ppm at 300 K), strongly indicating significant changes in pore environments for the sample that underwent multiple lithiation–delithiation cycles. At 173 K, both spectra show broad peaks with chemical shifts of 74 and 89 ppm for the CYC1 and CYC2, respectively. Higher chemical shift values associated with the smaller pores formed in CYC2 are most likely to arise from either the aggregates of broken-down particles or from the void of cracks in the existing SEI layers after multiple cycling. However, it is surprising to observe the presence of another peak at a lower chemical shift for CYC2 that is absent for all other samples. This additional peak at 6.5 ppm (see CYC2 spectra in Fig. 4) appears to be visible at temperatures at >173 K and the associated chemical shift did not

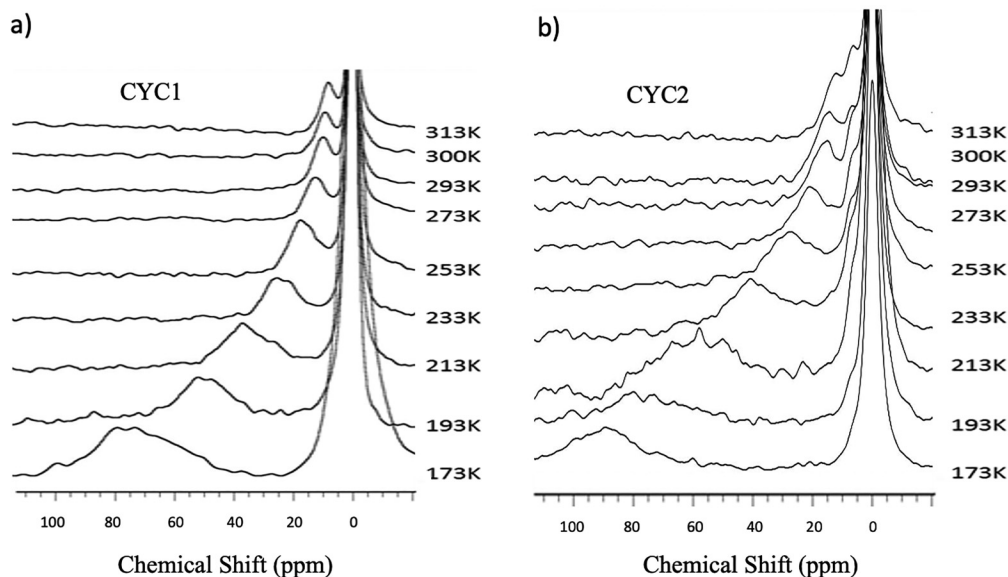


FIG. 4. Temperature-dependent HP ^{129}Xe NMR spectra taken for cycled composite Si electrodes: (a) CYC1 (cycled one time) and (b) CYC2 (cycled five times).

05 September 2023 11:38:23

change much with varying temperatures. The observation of two discernable resonance peaks at temperatures up to 313 K suggests that the relatively larger pores associated with this resonance peak at 6.5 ppm are not well connected with the smaller pores observed at higher chemical shifts. If these larger pores at 6.5 ppm are well connected to those smaller pores, the chemical shift observed for these larger pores would shift to higher ppm values as decreasing the temperatures due to the averaging of the signals from large and small pores. These smaller pores or cracks associated with the higher chemical shift might be partially blocked as a result of the formation of thick SEI layers upon multiple electrochemical cycling, inhibiting Xe diffusion from large pores to smaller pores.³⁷

Temperature-dependent ¹²⁹Xe NMR chemical shift data can be used to extract the physical adsorption of Xe on the pore surfaces based on Henry's law.³⁴ The relationship of the chemical shifts as a function of temperature is illustrated in Eq. (2) assuming the fast exchange and weak adsorption,

$$\delta = \delta_s \left(1 + \frac{B}{R\sqrt{T}} e^{-\frac{\Delta H_{ads}}{RT}} \right)^{-1}, \quad B = \frac{V_g}{SK_0}. \quad (2)$$

In Eq. (2), V_g , T , and S represent a free volume inside porous materials, a temperature, and a specific surface area, respectively, while K_0 , R , and ΔH_{ads} denote a pre-exponential term of Henry's constant K ,^{33–39} a universal gas constant, and heat of adsorption, respectively. δ_s is the chemical shift that is a characteristic of a given pore surface and can be estimated by the chemical shift observed at the lowest temperature before Xe starts to condense onto the surface at about 180 K under the CF conditions. Figure 5 displays the experimental data taken for unsoaked, soaked, SEI, and CYC1 samples along with the fitted temperature-dependent chemical shift curves using Eq. (2). It is clear from Fig. 5 that the experimental data are in good agreement with the fitted curve generated using Henry's law equation, indicating the adsorbed Xe in

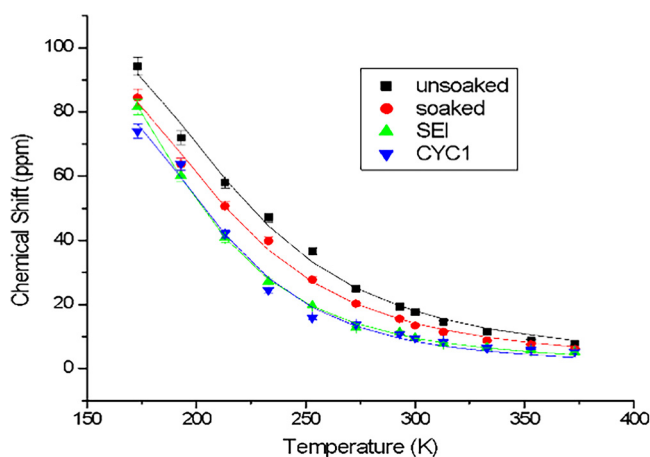


FIG. 5. Temperature-dependent chemical shift plots for unsoaked, soaked, SEI, and CYC1 composite Si electrodes. The dots are experimental data, and the dashed lines are fitted data along with the error bars.

TABLE II. Heat of adsorption and surface chemical shift values.

Si electrode	ΔH_{ads} (KJ/mol)	δ_s (ppm)
Unsoaked	13.0 ± 0.2	109 ± 1.3
Soaked	13.2 ± 0.1	104 ± 1.5
SEI	13.2 ± 0.3	95.59 ± 1.3
CYC1	15.0 ± 0.3	91.91 ± 1.3

nanocomposite electrode materials under experimental conditions in this study obeyed Henry's law at all temperatures.

ΔH_{ads} and δ_s values listed in Table II were obtained from fitting the variable temperature chemical shift data using Eq. (2). The results from the fitted data can only be useful for the qualitative comparison among different samples since Henry's law equation is mostly suitable for the well-defined pores with narrow pore size distribution. However, in this study, the situation is more complex. The pores here are mostly the void space from the aggregates of nanoparticles, unlike other well-defined pores. Thus caution has been exercised when interpreting the results quantitatively.^{34–39} Similar values of the heats of adsorption, ΔH_{ads} , were observed in Table II suggesting typical physical adsorption of Xe on surfaces for all measured samples. The δ_s values of 109 and 104 ppm listed in Table II for unsoaked and soaked samples decreased to 91–95 ppm for the SEI and CYC1 samples. Since δ_s depends on the chemical compositions of the pore surfaces and the geometries of the pores, it is understandable that obvious changes in chemical shifts occurred upon the formation of SEI layers causing the very different chemical composition of the pore surfaces for the SEI and CYC1 samples as compared with those unsoaked and soaked samples with no SEI.

D. Cycling effect on porosity and integrity of composite electrodes

A schematic illustration is given in Fig. 6 to explain the effect of cycling on porosity and the integrity of nanocomposite Si electrodes. However, caution has been taken in viewing Fig. 6 since a simplified model was used for the illustration. Figure 6 displays that

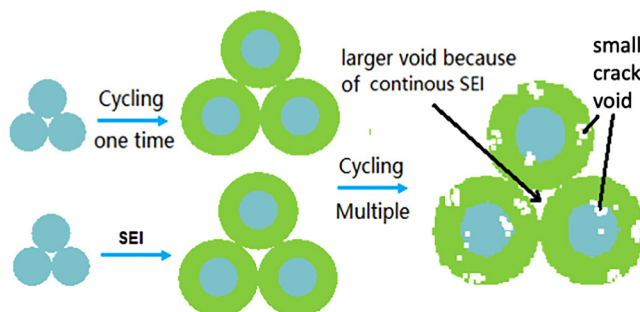


FIG. 6. Schematic illustration of the formation of SEI and cycling induced mechanical instability (e.g., cracking, voids) in composite Si electrodes.

the pores are the void spaces made of nanoparticle aggregates. The size of the pores is enlarged when SEI layers are formed on the Si nanoparticle surface due to the increased particle size. The SEI layer thickness was estimated to be ~ 18 nm at maximum based on our previous study.²⁹ The larger interparticle spacings as a result of the SEI growth contributed to the lower chemical shift observed in the ^{129}Xe NMR spectra of SEI, CYC1, and CYC2 samples in Figs. 1 and 3. Drawing of nearly identical particle size and interparticle spacings in Fig. 6 for SEI and CYC1 samples is based on the similar temperature-dependent ^{129}Xe NMR spectra (in Figs. 1 and 3). Figure 6 further illustrates that the porosity and connectivity in nanocomposite electrodes are not affected and the electrode is mostly intact after one lithiation–delithiation cycle. However, quite a different picture for the sample after multiple lithiation–delithiation cycles is depicted in Fig. 6, where a thicker SEI layer or larger particles are formed along with many small cracks in the SEI layer. This scenario is in agreement with the coexistence of two types of pores derived from combined ^{129}Xe and ^7Li NMR results for the multiple cycled sample (i.e., CYC2).

The illustration of increased voids among these enlarged particles is due to the formation of a thicker SEI layer for the CYC2 sample in comparison to SEI and CYC1 samples. This is supported by the observation of a lower chemical shift resonance peak at 6.5 ppm (Figs. 1 and 4) while the drawing of smaller pores inside these large particles is based on the observation of a second ^{129}Xe resonance peak at a higher chemical shift for the CYC2 sample. The thickening of the SEI layer in the multiple cycled sample is further validated by the fact that a significantly higher lithium content was found from the ^7Li NMR spectra (Fig. 2 and Table I). However, in reality, the situation is expected to be more complicated than the simplified schematic in Fig. 6. For example, there may be a case where an entire Si particle is completely broken down into smaller pieces after multiple cycling thereby creating smaller interparticle spacing or voids. However, this is an unlikely scenario as nanoparticles of Si are more robust than micrometer-sized particles to combat the lithiation–delithiation-induced volume changes. Some Si nanoparticles may develop small cracks as a result of multiple cycling. Depending on the depth of cracks, the deeper cracks in SEI may expose fresh Si surface to the electrolyte solution, resulting in further electrolyte reduction to form fresh SEI. The dynamic process of damage and repair of SEI with lithiation–delithiation cycles may also contribute to a gradual increase of Li^+ residue in silicon electrodes and to the increased thickness of the SEI layer. It is known that the thickening of SEI leads to poor cycling performance due to the combined effect of permanent Li loss, reduced lithium-ion diffusion, and increased mechanical stress from a thick SEI layer.^{40–43} The SEI layer is estimated to be ~ 18 nm thick after one lithiation–delithiation cycle using the same electrolyte from our previous study,²⁹ consequently, based on the present measurements, the thickness of SEI after multiple cycling is expected to be larger than 18 nm.

Based on the comparison of the chemical shifts observed in this study to those reported in our previous study,²⁹ a rough estimate of the smaller pore size formed in the CYC2 sample is ~ 10 Å or ~ 1 nm, much smaller than the interparticle spacing of SEI covered Si nanoparticles as illustrated in Fig. 6. Thus, it is reasonable to assume that the cracks of about 1–2 nm in depth are likely

to form inside the thick SEI layer (estimated to be >18 nm) after multiple cycling. Therefore, Fig. 6 paints a fairly clear picture of the fact that smaller voids or pores in the CYC2 sample most likely arise from the cracks in the thickened SEI layer rather than from the interparticle spacings between smaller broken-down Si particles. Our simple model illustrates that the porosity and the integrity of the electrode are significantly changed after multiple lithiation–delithiation cycles consistent with the changes in both ^{129}Xe and ^7Li NMR spectra. The results from this study demonstrate that a combination of ^{129}Xe and ^7Li NMR spectroscopy is a powerful diagnostic tool for monitoring the subtle changes in the early stages of electrode degradation and the mechanical failure in these Si nanocomposite electrodes after prolonged cycling and should prove valuable in designing composite electrodes with superior mechanical integrity/stability.⁴⁰

IV. CONCLUSIONS

Temperature-dependent HP ^{129}Xe NMR and ^7Li NMR spectroscopies have been successfully applied to examine the changes in the thickness of SEI layers, pore uniformity, and connectivity among different pores in nanocomposite Si electrodes upon electrochemical cycling. It was found that the initially formed SEI layer remains mostly intact after the first lithiation–delithiation, whereas multiple cycling induces SEI layer thickening and cracking in the SEI layer. In this study, HP ^{129}Xe NMR in combination with ^7Li NMR has been proven as a powerful tool in providing unique information on the microstructural (i.e., uniformity of the pores, pore connectivity) evolution in composite electrodes upon electrochemical cycling, complementary to other techniques. The results from this study help provide insight toward building more reliable and higher energy density nanocomposite electrodes for Li-ion batteries.

ACKNOWLEDGMENTS

The HP ^{129}Xe NMR work was supported by the EPSCoR Implementation Grant DE-SC0007074, Office of Basic Energy Sciences, and United States Department of Energy (U.S. DOE). The authors are grateful for the Advance Grant HRD-0548311 for purchasing parts of the equipment. L.-Q. Wang would like to dedicate this publication to commemorate the career of Dr. David Arthur Shirley, who was her Ph.D. thesis advisor whom she is deeply indebted to for his kindness, support, and guidance during her graduate school years at UC Berkeley.

AUTHOR DECLARATIONS

Conflict of Interest

The authors have no conflicts to disclose.

Author Contributions

Y.M. and N.K.K. contributed equally to this work.

DATA AVAILABILITY

The data that support the findings of this study are available from the corresponding author upon request.

REFERENCES

- ¹B. A. Boukamp, G. C. Lesh, and R. A. Huggins, *J. Electrochem. Soc.* **128**, 725 (1981).
- ²L. Y. Beaulieu, K. W. Eberman, R. L. Turner, L. J. Krause, and J. R. Dahn, *Electrochem. Solid-State Lett.* **4**, A137 (2001).
- ³S. D. Beattie, D. Larcher, M. Morcrette, B. Simon, and J.-M. Tarascon, *J. Electrochem. Soc.* **155**, A158 (2008).
- ⁴J. Yang, M. Winter, and J. O. Besenhard, *Solid State Ionics* **90**, 281 (1996).
- ⁵D. Munao, J. W. M. van Erven, M. Valvo, E. Garcia-Tamayo, and E. M. Kelder, *J. Power Sources* **196**, 6695 (2011).
- ⁶J. Li, R. B. Lewis, and J. R. Dahn, *Electrochem. Solid-State Lett.* **10**, A17 (2007).
- ⁷J. Yang, B. F. Wang, K. Wang, Y. Liu, J. Y. Xie, and Z. S. Wen, *Electrochem. Solid-State Lett.* **6**, A154 (2003).
- ⁸M. Kaneko, M. Nakayama, and M. Wakihara, *J. Solid State Electrochem.* **11**, 1071 (2007).
- ⁹H. M. Holzapfel, F. Krumeich, C. Veit, and P. Novák, *J. Power Sources* **161**, 617 (2006).
- ¹⁰W.-R. Liu, M.-H. Yang, H.-C. Wu, S. M. Chiao, and N.-L. Wu, *Electrochem. Solid-State Lett.* **8**, A100 (2005).
- ¹¹J. Drofenik, M. Gaberscek, R. Dominko, F. W. Poulsen, M. Mogensen, S. Pejovnik, and J. Jamnik, *Electrochim. Acta* **48**, 883 (2003).
- ¹²A. Magasinski, B. Zdyrko, I. Kovalenko, B. Hertzberg, R. Burtovyy, C. F. Huebner, T. F. Fuller, I. Luzinov, and G. Yushin, *ACS Appl. Mater. Interfaces* **2**, 3004 (2010).
- ¹³M. Wu *et al.*, *J. Am. Chem. Soc.* **135**, 12048 (2013).
- ¹⁴M. Nie, D. P. Abraham, Y. Chen, A. Bose, and B. L. Lucht, *J. Phys. Chem. C* **117**, 1257 (2013).
- ¹⁵B. Philippe, R. Dedryvere, J. Allouche, F. Lindgren, M. Gorgoi, H. Rensmo, D. Gonbeau, and K. Edstrom, *Chem. Mater.* **24**, 1107 (2012).
- ¹⁶D. E. Arreaga-Salas, A. K. Sra, K. Roodenko, Y. J. Chabal, and C. L. Hinkle, *J. Phys. Chem. C* **116**, 9072 (2012).
- ¹⁷J. H. Trill, C. Q. Tao, M. Winter, S. Passerini, and H. Eckert, *J. Solid State Electrochem.* **15**, 349 (2011).
- ¹⁸R. Elazari, G. Salitra, G. Gershinshy, A. Garsuch, A. Panchenko, and D. Aurbach, *J. Electrochem. Soc.* **159**, A1440 (2012).
- ¹⁹N. S. Choi, K. H. Yew, K. Y. Lee, M. Sung, H. Kim, and S. S. Kim, *J. Power Sources* **161**, 1254 (2006).
- ²⁰H. Nakai, T. Kubota, A. Kita, and A. Kawashima, *J. Electrochem. Soc.* **158**, A798 (2011).
- ²¹Y. M. Lin, K. C. Klavetter, P. R. Abel, N. C. Davy, J. L. Snider, A. Heller, and C. B. Mullins, *Chem. Commun.* **48**, 7268 (2012).
- ²²I. L. Moudrakovski, C. I. Ratcliffe, and J. A. Ripmeester, *J. Am. Chem. Soc.* **123**, 2066 (2001).
- ²³J. A. Ripmeester, *J. Am. Chem. Soc.* **104**, 289 (1982).
- ²⁴T. Ito and J. Fraissard, *J. Chem. Phys.* **76**, 5225 (1982).
- ²⁵C. I. Ratcliffe, *Annu. Rep. NMR Spectrosc.* **36**, 124 (1998).
- ²⁶B. C. Grover, *Phys. Rev. Lett.* **40**, 391 (1978).
- ²⁷W. Happer, E. Miron, S. Schaefer, D. Schreiber, W. A. Van Wingen, and X. Zeng, *Phys. Rev. A* **29**, 3092 (1984).
- ²⁸B. Driehuis, G. D. Cates, E. Miron, K. Sauer, D. K. Walter, and W. Happer, *Appl. Phys. Lett.* **69**, 1668 (1996).
- ²⁹Y. Mao, N. Karan, M. Song, R. Hopson, P. Guduru, and L.-Q. Wang, *Energy Fuels* **31**, 5622 (2017).
- ³⁰I. C. Ruset, S. Ketel, and F. W. Hersman, *Phys. Rev. Lett.* **96**, 053002 (2006).
- ³¹G. Schrank, Z. Ma, A. Schoeck, and B. Saam, *Phys. Rev. A* **80**, 063424 (2009).
- ³²L.-Q. Wang, "Hyperpolarized 129Xe NMR in materials sciences: Pore structure, interconnectivity, and functionality," in *Hyperpolarized Xenon-129 Magnetic Resonance: Concepts, Production, Techniques, and Applications* (RSC Publishing, London, 2015).
- ³³Y. Mao, M. Song, R. Hopson, N. K. Karan, P. R. Guduru, and L.-Q. Wang, *Energy Fuels* **30**, 1470 (2016).
- ³⁴V. Tersikh, I. Moudrakovskii, and V. Mastikhin, *J. Chem. Soc. Faraday Trans.* **89**, 4239 (1993).
- ³⁵J. A. Ripmeester and C. I. Ratcliffe, *J. Phys. Chem.* **94**, 7652 (1990).
- ³⁶I. L. Moudrakovski, V. V. Tersikh, C. I. Ratcliffe, J. A. Ripmeester, L.-Q. Wang, Y. Shin, and G. J. Exarhos, *J. Phys. Chem. B* **106**, 5938 (2002).
- ³⁷L.-Q. Wang, D. Wang, L. Liu, G. Exarhos, J. S. Pawsey, and I. Moudrakovski, *J. Phys. Chem. C* **113**, 6577 (2009).
- ³⁸L.-Q. Wang, D. Wang, L. Liu, and G. J. Exarhos, *J. Phys. Chem. C* **116**, 22 (2012).
- ³⁹V. V. Tersikh, I. L. Moudrakovski, S. R. Breeze, S. Lang, C. I. Ratcliffe, J. A. Ripmeester, and A. Sayari, *Langmuir* **18**, 5653 (2002).
- ⁴⁰J. D. McBrayer, C. A. Apblett, K. L. Harrison, K. R. Fenton, and S. D. Minter, *Nanotechnology* **32**, 502005 (2021).
- ⁴¹A. Tokranov, B. W. Sheldon, C. Z. Li, S. Minne, and X. C. Xiao, *ACS Appl. Mater. Interfaces* **6**, 6672 (2014).
- ⁴²W. Zhang, T. H. Cai, and B. W. Sheldon, *Adv. Energy Mater.* **9**, 1803066 (2019).
- ⁴³K. Guo, R. Kumar, X. C. Xiao, B. W. Sheldon, and H. J. Gao, *Nano Energy* **68**, 104257 (2020).

05 September 2023 11:38:23